Click Here for Full Article

Influence of surrounding plates on 3D subduction dynamics

P. Yamato,[1] L. Husson,[1] J. Braun,[1] C. Loiselet,[1] and C. Thieulot[2]

[1] Our 3D modelling study shows that the presence of lithospheric plates around a subducting plate has a significant influence on subduction dynamics, in particular on trench retreat rate, slab dip, and lateral shortening of the subducting plate. Neighbouring plates prevent unrealistic plate behaviour with no need for complex rheologies. Because, at the Earth's surface, plates form a continuous shell, they should not be neglected. **Citation:** Yamato, P., L. Husson, J. Braun, C. Loiselet, and C. Thieulot (2009), Influence of surrounding plates on 3D subduction dynamics, *Geophys. Res. Lett.*, *36*, L07303, doi:10.1029/2008GL036942.

1. Introduction

[2] At the Earth's surface, tectonic plates form a complete shell and, therefore, no plate can be considered in isolation. A "complete" subduction system is thus made of four plates: the subducting, overriding and lateral plates.

[3] A variety of models have been proposed, using physical [e.g., *Bellahsen et al.*, 2005; *Funiciello et al.*, 2003a, 2006, 2008; *Schellart*, 2008], semi-analytical [*Royden and Husson*, 2006] and numerical methods [e.g., *Stegman et al.*, 2006; *Clark et al.*, 2008] to study the dynamics of subduction zones in 3D. However most studies, with the exception of a few [e.g., *Zhong and Gurnis*, 1995; *Royden and Husson*, 2006; *Espurt et al.*, 2008; *Regard et al.*, 2008; *Clark et al.*, 2008; *Bonnardot et al.*, 2008], considered the subducting plate in isolation, by focusing on its interactions with the surrounding mantle. In cases where the overriding plate is not included, one commonly assumes that it has no effect on mantle flow since it passively accompanies the retreating trench [*Bellahsen et al.*, 2005; *Funiciello et al.*, 2003b].

[4] However, because plates are stiffer and denser than the upper mantle, the presence or absence of lithospheric material in the upper mantle influences the velocity field in and around a subducting plate, and the dynamics of subduction will depart from the "intrinsic" dynamics of an isolated subduction system. Both the poloidal (downdip, in a vertical plane) and toroidal (at the slab edges, in a plane parallel to the surface) components of the return flow induced by the motion of the slab in the viscous upper mantle is not limited to the deepest parts of the subduction system but also reaches the surface; this flow may affect the motion of other plates and conversely, be influenced by them.

[5] In most models where the subducting plate is considered in isolation, the plate is not prevented from flowing laterally by the presence of neighbouring plates, as it is in natural systems. The deformation of the edges of the plate naturally occurs in purely viscous models, a phenomena that seems to be fortuitously limited in physical models by the possible action of surface tension or by the elastic properties of the material used [e.g., *Schellart*, 2008]. To prevent this artificial lateral flow, several *ad hoc* parameterizations have been used, including using a very high viscosity contrast between the plate and surrounding mantle, incorporating plasticity through a yield strength that is sufficiently high to prevent the horizontal deformation but small enough to permit slab bending [e.g., *Moresi and Solomatov*, 1998; *Stegman et al.*, 2006], imposing an arbitrary cut-off for stress transmission [*Husson*, 2006], or adding elasticity [e.g., *Bonnardot et al.*, 2008].

[6] Herein we quantify the impact of surrounding plates on subduction dynamics through a series of simple experiments carried out using a 3D numerical model of linear viscous fluid flow. It is not our purpose here to explore the many parameters of the system (e.g., geometry of the lithosphere, boundary conditions, viscosity, or density ratios): we choose a given setup in all our experiments and focus on the influence of surrounding plates.

2. Model Setup

[7] We have used the 3D code *DOUAR* described in details by *Braun et al.* [2008], originally designed for thermo-mechanical modelling. In this study, we are interested in understanding the basic interactions of a subducting plate with the surrounding mantle and adjacent plates; we have thus used a linear viscous rheology for all components of the system, neglecting non-linear effects arising from the thermal and stress-dependence of rheology.

[8] The initial model and the material parameters (effective viscosity and density) are presented in Figure 1a. Since the YZ plan at $X = 0$ in our model is a plane of symmetry, we only model one half of the slab along the left-hand side ($X = 0$) of the 3D box, leaving enough space to its right (i.e., between $X = 0.5$ and $X = 1.0$) to prevent most boundary effects. In all experiments, the initial geometry corresponds to an ongoing, though immature, subduction zone. The size of the square unit model box corresponds to 3000 km. The upper/lower mantle boundary is characterized by a viscosity jump at 660 km. The crust and mantle lithosphere are respectively 30 and 120 km thick. We chose thick lithosphere and crust in order to preserve a high resolution (additional tests are performed with thicknesses that are twice thinner). The resolution of the model is ∼25 km between the top of the model and the upper-lower mantle boundary, where most of the deformation occurs, and 50 km elsewhere. The resolution is further improved by the *divFEM* algorithm used in *DOUAR* that can be tailored to represent density variations at an even smaller scale (∼6 km)

[1] Geosciences Rennes, UMR6118, Université de Rennes 1, CNRS, Rennes, France.

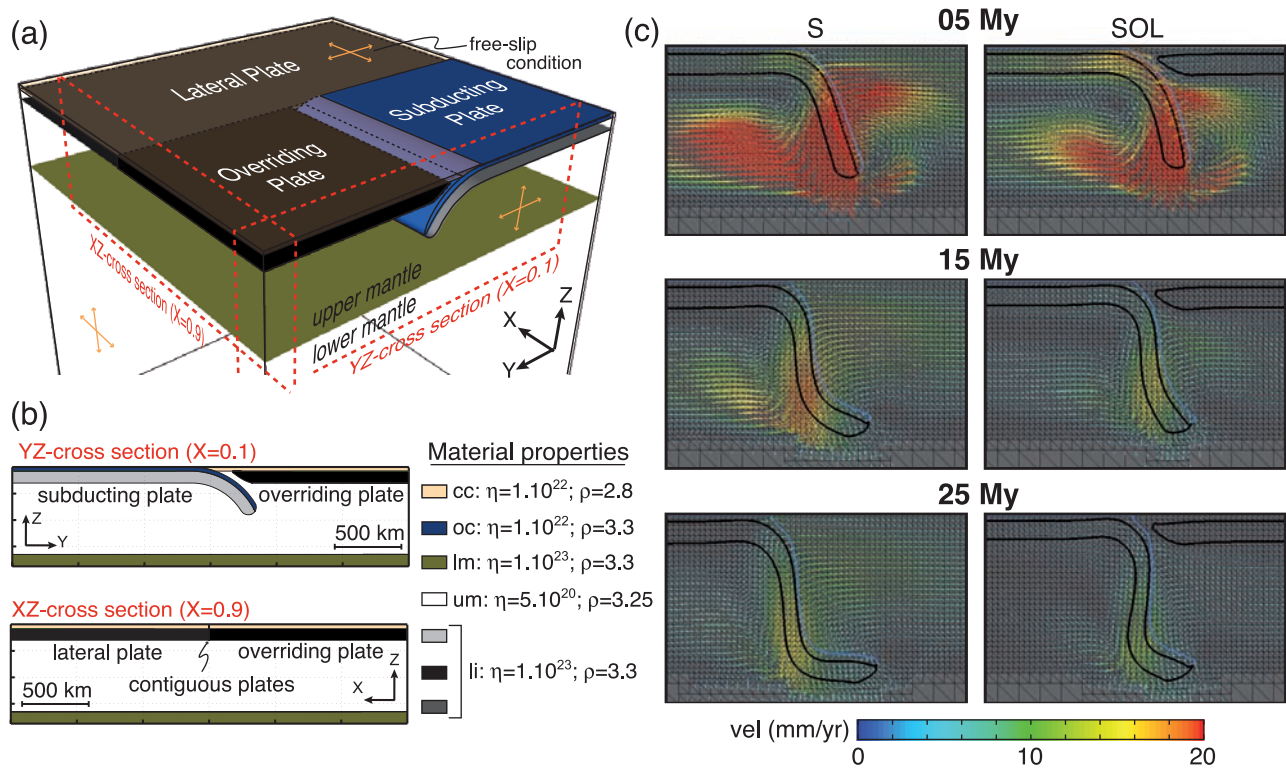[2] Department of Earth Sciences, Bergen University, Bergen, Norway.

Figure 1. (a) 3D view of the model box at the beginning of the experiment. (b) Cross-sections showing plate stratification (crust and mantle) and material properties. *oc* and *cc*, oceanic and continental crust, *li*, *um* and *lm*: lithospheric, upper and lower mantle. Black, dark grey and light grey indicate overriding, lateral and subducting mantle lithosphere, respectively. (c) Subduction evolution during 25 My for the two models *S* and *SOL*. (YZ Cross-section taken at X = 0.1 corresponding to 300 km, see Figure 1a).

[*Braun et al.*, 2008]. Four configurations, that include respectively the Subducting plate only (S), the Subducting and Overriding plates only (SO), the Subducting and Lateral plates only (SL), and all plates together (SOL), were tested (Figure 1a). All models are nonetheless everywhere capped by a relatively buoyant, moderate viscosity crust, which in turns decreases the phenomena described below (e.g., trench retreat, lateral shortening and subduction).

[9] Material densities and viscosities are scaled to the upper mantle reference values (Figure 1b). In nature, the effective viscosity ratio between the subducting lithosphere and the upper mantle is thought to be in the range of 10 to 10^3 [e.g., *Hager*, 1984; *Davies and Richards*, 1992; *Mitrovica and Forte*, 2004]. We have thus used a viscosity ratio of 200, which also is a commonly used value that predicts realistic kinematics [e.g., *Funiciello et al.*, 2003a; *Schellart*, 2004, *Stegman et al.*, 2006, *Schellart*, 2008]. The lower mantle to lithosphere viscosity ratio is set to 1, high enough to limit slab penetration across the 660 km discontinuity. A crustal layer with a scaled viscosity of 20 caps the entire model; its scaled density is 1.015 over the subducting lithosphere and 0.8615 everywhere else (continental crust). All lithospheric mantle units are also contiguous, except for a rectangular gap between the subducting and the overriding lithosphere, where low viscosity material with upper mantle rheology facilitates the subduction process (Figure 1b). The crustal layer controls the kinematics [e.g., *Royden and Husson*, 2006] but the nature of this control is beyond our scope and we assign density and viscosity values that

predict subduction velocities of a few mm.yr^{-1} (*v*-velocity component on Figure 2). Free-slip boundary conditions are imposed on all sides of the model and plate motion is resisted by the no-velocity conditions imposed at the plate boundaries (fixed plates, Figure 1a).

[10] This is an end-member situation in order to characterise the largest possible effect. Three-dimensional dynamic modelling of subduction zones is most relevant for small subduction zones. The behaviour of many small-sized subduction zones can thus be best approximated by the "fixed plate" setup we have used here, because their subduction rate is much faster than the plate convergence rate (e.g., Scotia, Hellenic, Tyrrhenian, Calabria…). We performed a few experiments with a free upper surface (no stress), but this required a much larger number of small time steps and did not lead to significantly different conclusions.

3. General Evolution of the Models

[11] In all experiments the subduction process evolves in three stages (Figure 1c) [see also *Bellahsen et al.*, 2005; *Stegman et al.*, 2006]: (1) the slab sinks in the upper mantle, (2) approaches the upper-lower mantle discontinuity and bends, (3) the slab tail (i.e., the bottom end of the slab) rests on the upper/lower mantle discontinuity and the system reaches a steady-state where further subduction is accompanied by trench retreat. The first sinking stage can be polluted by the initial geometry but can be assimilated to the transient stage existing between subduction initiation and
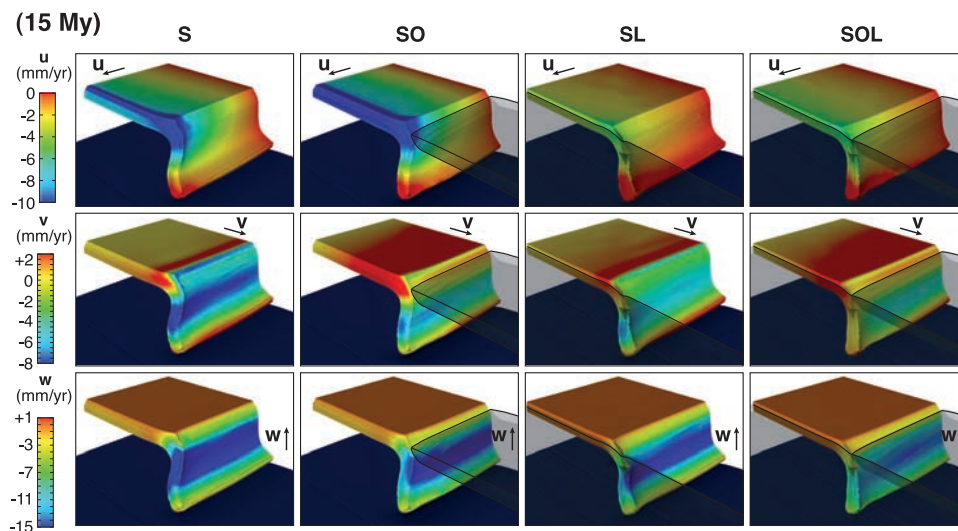
Figure 2. Velocity field components for the subducting plate for each experiment after 15 Myr. The shapes of the lateral and overriding lithospheres are presented as ghosts (the crust on the overriding and lateral plate is not shown).

'steady state' subduction. Trench retreat takes place when the slab approaches the 660 km discontinuity (stage 2), after an initial stage of advance (Figure 3a).

[12] In our models, the crust is advected in depth with the subducting lithosphere following the velocity field. The channel between the subducting and the overriding plates can thus evolve freely. The poloidal component of mantle flow is attenuated as the slab approaches the 660 km discontinuity (Figure 1c) because the upper mantle can no longer flow beneath the slab tail and the lower mantle.

[13] At intermediate depths (i.e., between 275 and 375 km), the slab dip is broadly similar in all experiments. During the first stage, slab dip increases from $60°$ to $\sim 75-80°$. In stage 2, it remains stable as the slab approaches the 660 km discontinuity, before increasing again during the bending of the slab tail along the 660 km discontinuity. In all experiments steady state is reached after ~ 20 Myr, with slab dips at intermediate depths ranging between $83°$ and $92°$. The *SOL* and *SO* experiments display steeper slabs than in the *S* and *SL* experiments where slab dip is always lower than $90°$.

4. Slab Rollback and Trench Retreat

[14] Subduction is accompanied by a faster rate of trench retreat in the experiments where the overriding plate is absent (y-component of the velocity field (*v*), mid. panel, Figure 2). This is illustrated in details in Figures 3a and 3b where the location (Figure 3a) and velocity (*v*-component, Figure 3b) of the trench are given as a function of time. Horizontal velocities, strain rates and deviatoric stresses along cross-sections from the models S and SOL are also given in the auxiliary material with description.[1]

[15] The poloidal flow induced by the sinking slab is made of two cylindrical cells, on either side of the slab. When the overriding plate is absent (Figure 1c), the cell in

front of the slab extends from the slab tail to the surface. When the more viscous overriding plate is present, it does not extend to the surface but is limited to the base of the overriding plate. This difference influences subduction dynamics in two important ways. First, in the absence of overriding plate (*S* and *SL* experiments), the return flow amplifies trench retreat rates (Figure 2) by a factor of 2 to 5 (Figure 3b), as opposed to experiments with an overriding plate (*SO* and *SOL* experiments). Consequently, slab retreat rate will always be overestimated in experiments where the overriding plate is not accounted for. Secondly, the maximum velocity generated by the poloidal flow found at the top of the upper mantle, i.e. deeper with an overriding plate, explains the slightly higher slab dip values in *SO* and *SOL* than in *S* and *SL* (Figure 2).

5. Lateral Behaviour of the Subducting Plate

[16] Let's now consider the evolution of the slab in the third dimension (along the X axis, Figures 2, 3c, and S1). In both the *S* and *SO* experiments, the lateral edge of the subducting plate is not held by another plate alongside and is affected by trench parallel shortening (Figure 2, top). Significant shortening occurs for models with no lateral plate (Figure 3d) and is partly caused by subduction along the side of the subducting plate, driven by the negative buoyancy of the plate. The fact that the plate is fixed at the boundary induces additional extension on the plate, which stretches accordingly along the y-direction; this stretching has to be compensated by shortening along the x- and z-directions. Shortening is facilitated when the plate is not maintained laterally (*S* and *SO* experiments). After 20 Myr, total shortening values obtained are 3 times greater for the *S* and *SO* experiments ($\sim 15\%$) than for *SL* and *SOL* ($\sim 5\%$). As illustrated in Figure 3e where the maximum depth of the subducting plate measured along its edge is shown as a function of time for each of the four experiments, the presence of the neighbouring plate prevents shortening and thus the lateral subduction of the subducting plate.
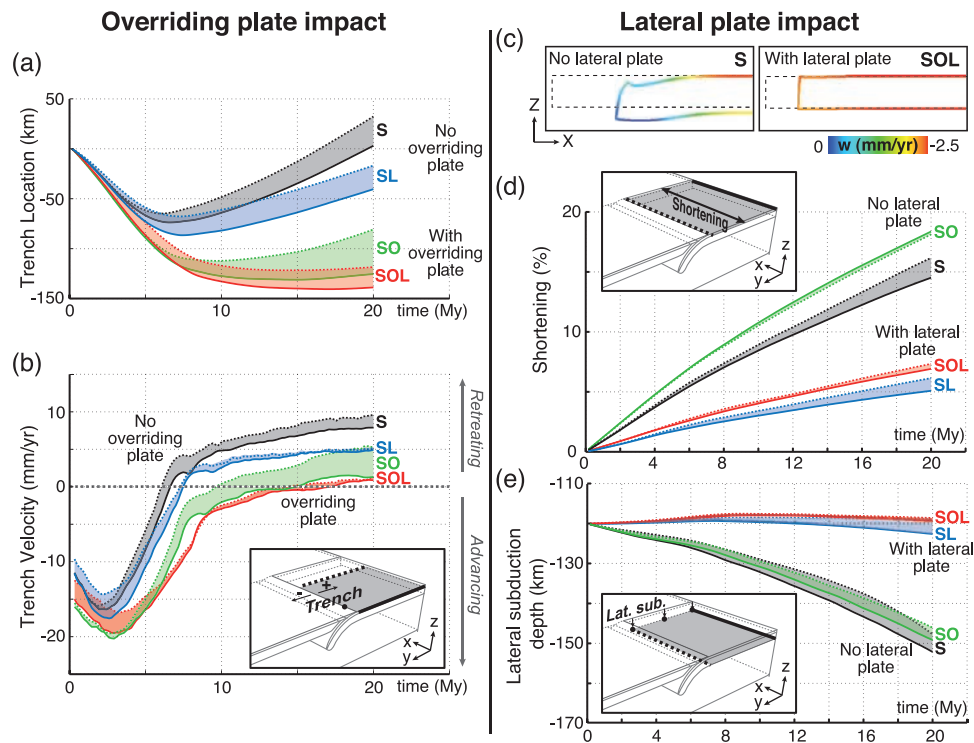
Figure 3. (a) Trench location and (b) velocity through time. Solid and dashed lines correspond to values calculated respectively at X = 0 and X = 0.35 (1050 km) from the right side of the model box (see inset). (c) Lateral behavior of the subducting lithosphere for the two models S and SOL after 20 Myr (XZ cross-section at Y = 0.1). Dashed and color lines correspond to the location of the subducting plate at t = 0 Myr and t = 20 Myr. (d) Lateral shortening of the subducting plate. (e) Maximum depth of lateral subduction (lat. sub.) reached by the lateral edge of the subducting plate. Solid and dashed lines correspond to the values at Y = 0 and Y = 0.4 (1200 km) from the backside of the model box (see inset).

Indeed, after 20 Myr, the plate edge has penetrated into the upper mantle to a depth of ∼150 km for *S* and *SO* (Figure 3e), whereas it has remained at its initial depth when a lateral plate is included (*SL* and *SOL*, Figure 3c). Although the subducting lithosphere is equally gravitationally unstable in all four experiments and has thus the same tendency to subduct on all sides, the presence of a lateral plate reduces the negative buoyancy and thus prevents lateral subduction.

6. Conclusion and Discussion

[17] Surrounding plates in subduction systems affect the global dynamic of the subduction process in multiple ways. (1) The presence of an overriding plate modifies the poloidal flow generated by a subducting slab. Consequently, neglecting overriding plate leads to overestimating trench retreat velocities by a factor 2 to 5 and underestimating slab dips at depth. (2) The presence of a lateral plate prevents lateral shortening observed in many experiments where the subducting plate is considered in isolation; a phenomenon that leads to models including complex rheologies that prevent such undesirable effects [e.g., *Moresi and Solomatov*, 1998; *Stegman et al.*, 2006]. As previously shown [e.g., *King and Hager*, 1990; *Conrad and Hager*, 1999], 3D models composed of a single plate predict subduction velocities that have to be considered as upper bound values. However, in a purely viscous system, our experiments show that the absence of lateral plates leads to unrealistic lateral shortening and to the lateral subduction of the plate, which is not observed in natural subduction zones. Studies that do not account for the presence of surface plates may provide qualitative information that is only valid under the assumption that surrounding plates are weak (oceanic subduction in the presence of a well developed back-arc system, for instance). Our setup assumes that the plates are pinned to the sidewalls. When plates are "free", these effects are significantly reduced but still important. In real Earth, most small-scale subduction zones, for which our setup is relevant, are characterized by subduction rates that are much faster than the plate convergence rate (i.e., they are "fixed"). In addition, the large model crustal and mantle lithosphere thicknesses seemingly enhance our results. However, because the model is Newtonian, assigning thinner lithosphere and crust leads to comparable results for a given amount of subduction (not for a given time), as confirmed by additional tests.

[18] Our results suggest that all plates must be included in modelling-based studies, where the effects of many parameters characterizing a subduction system (e.g., lithosphere thickness, viscosity and density ratios, friction between plates, velocity/stresses boundary conditions…) are explored.

References

Bellahsen, N., C. Faccenna, and F. Funiciello (2005), Dynamics of subduction and plate motion in laboratory experiments: Insights into the "plate tectonics" behavior of the Earth, *J. Geophys. Res.*, *110*, B01401, doi:10.1029/2004JB002999.

Bonnardot, M. A., R. Hassani, E. Tric, E. Ruellan, and M. Régnier (2008), Effect of margin curvature on plate deformation in a 3-D numerical model of subduction zones, *Geophys. J. Int.*, *173*, 1084–1094, doi:10.1111/j.1365-246X. 2008.03752.x.

Braun, J., C. Thieulot, P. Fullsack, M. DeKool, C. Beaumont, and R. Huismans (2008), DOUAR: A new three-dimensional creeping flow numerical model for the solution of geological problems, *Phys. Earth Planet. Inter.*, *171*, 76–91, doi:10.1016/j.pepi.2008.05.003.

Clark, S. R., D. Stegman, and R. D. Müller (2008), Episodicity in back-arc tectonic regimes, *Phys. Earth Planet. Inter.*, *171*, 265–279, doi:10.1016/j.pepi.2008.04.012.

Conrad, C. P., and B. H. Hager (1999), Effects of plate bending and fault strength at subduction zones on plate dynamics, *J. Geophys. Res.*, *104*, 17,551–17,571.

Davies, G. F., and G. F. Richards (1992), Mantle convection, *J. Geol.*, *100*, 151–206.

Espurt, N., F. Funiciello, J. Martinod, B. Guillaume, V. Regard, C. Faccenna, and S. Brusset (2008), Flat subduction dynamics and deformation of the South American plate: Insights from analog modeling, *Tectonics*, *27*, TC3011, doi:10.1029/2007TC002175.

Funiciello, F., C. Faccenna, D. Giardini, and K. Regenauer-Lieb (2003a), Dynamics of retreating slabs: 2. Insights from three-dimensional laboratory experiments, *J. Geophys. Res.*, *108*(B4), 2207, doi:10.1029/2001JB000896.

Funiciello, F., G. Morra, K. Regenauer-Lieb, and D. Giardini (2003b), Dynamics of retreating slabs: 1. Insights from two-dimensional numerical experiments, *J. Geophys. Res.*, *108*(B4), 2206, doi:10.1029/2001JB000898.

Funiciello, F., M. Moroni, C. Piromallo, C. Faccenna, A. Cenedese, and H. A. Bui (2006), Mapping mantle flow during retreating subduction: Laboratory models analyzed by feature tracking, *J. Geophys. Res.*, *111*, B03402, doi:10.1029/2005JB003792.

Funiciello, F., C. Faccenna, A. Heuret, S. Lallemand, E. Di Giuseppe, and T. W. Becker (2008), Trench migration, net rotation and slab-mantle coupling, *Earth Planet. Sci. Lett.*, *271*, 233–240, doi:10.1016/j.epsl.2008.04.006.

Hager, B. H. (1984), Subducted slab and the geoid: Constraints on mantle rheology and flow, *J. Geophys. Res.*, *89*, 6003–6015.

Husson, L. (2006), Dynamic topography above retreating subduction zones, *Geology*, *34*, 741–744.

King, S. D., and B. H. Hager (1990), The relationship between plate velocity and trench viscosity in Newtonian and power-law subduction calculations, *Geophys. Res. Lett.*, *17*, 2409–2412.

Mitrovica, J. X., and A. M. Forte (2004), A new inference of mantle viscosity based upon joint inversion of convection and glacial isostatic adjustment data, *Earth Planet. Sci. Lett.*, *225*, 177–189, doi:10.1016/j.epsl.2004.06.005.

Moresi, L., and V. Solomatov (1998), Mantle convection with a brittle lithosphere: Thoughts on the global tectonic styles of Earth and Venus, *Geophys. J. Int.*, *133*, 669–682.

Regard, V., C. Faccenna, O. Bellier, and J. Martinod (2008), Laboratory experiments of slab break-off and slab dip reversal: Insight into the Alpine Oligocene reorganization, *Terra Nova*, *20*, 267–273.

Royden, L. H., and L. Husson (2006), Trench motion, slab geometry and viscous stresses in subduction systems, *Geophys. J. Int.*, *167*, 881–905.

Schellart, W. P. (2004), Quantifying the net slab pull force as a driving mechanism for plate tectonics, *Geophys. Res. Lett.*, *31*, L07611, doi:10.1029/2004GL019528.

Schellart, W. P. (2008), Kinematics and flow patterns in deep mantle and upper mantle subduction models: Influence of the mantle depth and slab to mantle viscosity ratio, *Geochem. Geophys. Geosyst.*, *9*, Q03014, doi:10.1029/2007GC001656.

Stegman, D. R., J. Freeman, W. P. Schellart, L. Moresi, and D. May (2006), Influence of trench width on subduction hinge retreat rates in 3-D models of slab rollback, *Geochem. Geophys. Geosyst.*, *7*, Q03012, doi:10.1029/2005GC001056.

Zhong, S., and M. Gurnis (1995), Mantle convection with plates and mobile, faulted plate margins, *Science*, *267*, 838–843.

———————————

J. Braun, L. Husson, C. Loiselet, and P. Yamato, Geosciences Rennes, UMR6118, Université de Rennes 1, CNRS, Bat. 15, F-35042 Rennes CEDEX, France. (philippe.yamato.rennes1@gmail.com)

C. Thieulot, Department of Earth Sciences, Bergen University, Allegaten 41, N-5007 Bergen, Norway.